

Molecular dynamics simulation of the interaction of 5-keto substituted 7-*tert*-butyl-2,3-dihydro-3,3-dimethylbenzofuran derivatives with cyclooxygenase-2

V. Kothekar*, S. Sahi and J. Mishra

Department of Biophysics, All India Institute of Medical Sciences, New Delhi 110 029, India

We present here results on molecular dynamics simulation of three 7-*tert*-butylbenzofurans with substituents at the fifth position: CONH(CH₂)₂OMe (BF1), CONH-c-Pr(cyclopropyl) (BF2) and 3-methylene-*g*-butyrolactonyl (BF3), complexed with cyclooxygenase-2 (COX-2), a target for non-steroidal anti-inflammatory drugs (NSAIDs). Perturbative changes in the enzyme structure, energetics of interaction and points of contact are monitored. Our results showed that difference in root mean square deviations (RMSDs) of backbone Ca atoms in inter-domain contact and heme binding loops, better interaction with adjoining helical segments, H-bonding and electrostatic interaction with Arg120, Tyr355, Arg513, His90 and more 'relaxed conformation' at the channel entrance led to better COX-2 selectivity by BF1. Hydrophobic contacts with Met113, Pro86 and Val89 increase COX-2 selectivity. Higher potency of BF3 is due to its better interaction with membrane-anchoring region of COX-2 and larger mobility of residues in the cavity.

5-keto substituted 7-*tert*-butyl-2,3-dihydro-3,3-dimethylbenzofurans (DHDMBFs) are anti-inflammatory and analgesic agents^{1,2}. With the substituents in the fifth position these are dual cyclooxygenase (COX) and 5-lipoxygenase (LOX) inhibitors. They inhibit both the isoforms of COX (COX-1 and COX-2). CONH(CH₂)₂OMe (BF1) is 60 and 2.5 times more selective than CONH-c-Pr(cyclopropyl) (BF2) and 3-methylene-*g*-butyrolactonyl (BF3), whereas BF3 has 10 and 180 times more potency than BF1 and BF2, respectively. COX-2 is known to occur in limited number of tissues and is regulated by specific stimuli³⁻⁵. It is responsible for prostanoid biosynthesis involved in inflammation and mitogenesis⁶. Its levels rise significantly during acute chronic inflammation in the presence of cytokines, mitogens and endotoxins in leukocytes⁷ and it is responsible for elevated levels of prostaglandins during inflammation^{4,8,9}. COX-1 is

assigned the 'housekeeping job'. It is important physiologically for maintenance of renal and gastric homeostasis¹⁰⁻¹². Its inhibition leads to gastrointestinal disorders. As a consequence, prolonged treatment by non-selective non-steroidal anti-inflammatory drugs (NSAIDs) gives undesirable side effects. The objective of the present work is to analyse mechanistic cause related to COX-2 selectivity and potency by DHDMBFs. The study would be helpful in design of more potent and less toxic NSAIDs.

The task is not easy, because of the topological similarity in the catalytic domains of COX-1 and COX-2 and occurrence of the same amino acid side chains in their active cavities¹³⁻¹⁸. As per genetic modification data¹⁹⁻²³, residues Arg120, Tyr355, Val509, Arg513, Ile523 and Glu524 are important for NSAIDs binding to COX-2 and its selective inhibition. The kinetic data²⁴⁻²⁸ showed that the major role in COX-2 selectivity is played by structural dynamics. However this could not be easily judged from available X-ray data because of their low resolution (2.9-3.2 Å). With increasing computational power and availability of simulation software, computer modelling gives a handy tool for studying enzyme inhibitor interactions. Our earlier studies^{29,30} on NS398 (a COX-2 selective inhibitor) and indoprofen (a nonselective COX inhibitor), with COX-1 and COX-2 showed interesting correlation amongst energetics, points of contact between the enzyme and inhibitor, ligand-induced perturbative changes in the enzyme and COX-2 selectivity and activity. Since NS398 and indoprofen belonged to different chemical series, we selected here DHDMBFs with different substituents at the fifth position (BF1, BF2 and BF3, Figure 1).

Methodology

The coordinates for BF1, BF2 and BF3 were obtained by energy minimization using bond length and bond angle data on indoprofen³¹. The charges on the atom centres needed for energy calculations were obtained by

*For correspondence. (e-mail: kothekar@medinst.ernet.in)

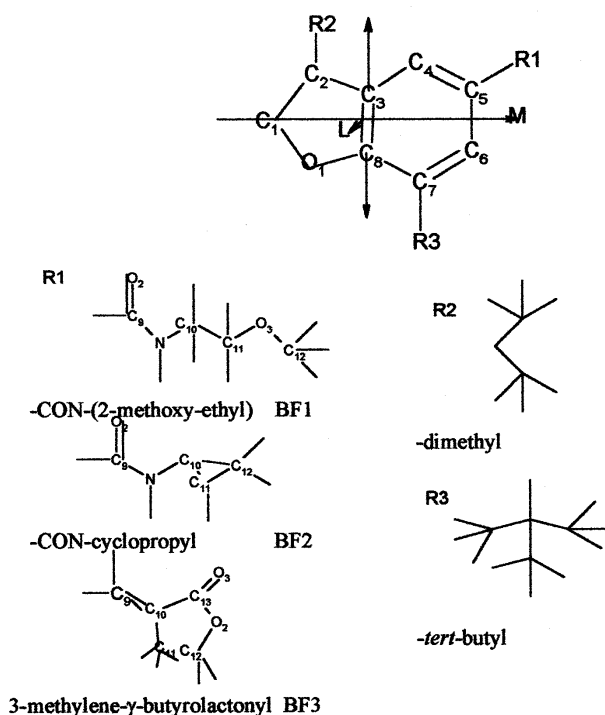


Figure 1. Nomenclature for DHDMBFs. Shown here are three mutually perpendicular axes, M, N and L used for complex modelling.

MOPAC 7.0 (ref. 32). The methodic details are described in our earlier paper³³. Structural models for complexes were obtained using 3D X-ray coordinates of flurbiprofen and SC558 with COX-2 (ref. 17) downloaded from Protein Data Bank³⁴. These two complexes were chosen because of similarity between DHDMBFs and these ligands. The benzene ring of the DHDMBFs was overlapped with the same of flurbiprofen. The *tert*-butyl group (chain R3) was oriented towards Tyr385. The carbonyl oxygen in BF1 and BF2 and CH of BF3 in the chain R1 were then brought in the vicinity of the fluorine atom of flurbiprofen, using the program MOLMOL³⁵. Ome of BF1 and *c*-propyl of BF2 were oriented in the direction of sulphonamide group of SC558. The drugs were then translated and rotated along axes L, M and N shown in Figure 1, using our program IMF1 (ref. 36). At each point the rotations were allowed along all the flexible bonds in side chain R1. Amino acid chains in the COX-2 cavity were kept flexible. The energy scoring was done using non-bonded, electrostatic and H-bond interactions calculated with AMBER force field parameters³⁷. For the sake of convenience, models of BF1, BF2 and BF3 complexed with COX-2 will be henceforth referred as **BF1**, **BF2** and **BF3**. Energy minimization and molecular dynamics simulations were carried out using Sander's module of AMBER 5.0 (ref. 37) with all-atom force field. For calculation of non-bonded interactions, we used 8 Å

cut-off distance. The list was upgraded after every 20 cycles. Hundred steps of steepest descent were followed by conjugate gradient minimization method³⁸ for 15,000 cycles. Potential energies of the complexes were -7435.8, -7308.7 and -7435.3 kcal/mole, respectively in **BF1**, **BF2** and **BF3** and predominantly electrostatic. Ligand-protein interaction energies were -38.5, -37.0 and -35.3 kcal/mol in **BF1**, **BF2** and **BF3**. Energy-minimized model of **BF1** is shown in Figure 2a and b using RASMOL³⁹. Integration was carried out using Verlet's⁴⁰ and Leap-Frog approximations⁴¹ with time step 0.001 picoseconds (ps). Heating from 10 to 300 K was achieved in 30 ps. The system was equilibrated for 110 ps. This was followed by simulation for 250 ps. Fifty-five coordinate files were pulled out at 0.1 ps time interval and sub-averaged for 2 ps during last 110 ps of simulation. Snapshots of molecular dynamics trajectories at 180 and 210 ps for **BF1** and **BF3** are depicted in Figure 2c and d. Structure-based parameters are analysed using MOLMOL³⁵ and ANALMD, an in-house package. The ligand volumes are calculated by dipping them in Monte Carlo-equilibrated water bath with TIP3P model⁴² and counting the number of displaced water molecules.

Results and discussions

The active cavities of COX-1 and COX-2 extend from the membrane-binding region (loop of residues 111–120), through a narrow entrance restricted by H-bonding network between side chains of Arg120, Glu524, Tyr355 and Arg513 (in case of COX-2) to Tyr385 at the apex of the channel. The heme group is located above Tyr385 (Figure 2a). Upper portion of the channel is occupied predominantly by hydrophobic residues. Lower portion has a mixture of neutral polar, basic and few hydrophobic amino acids. In COX-2, because of few amino acids changes (Ile523 to Val523 and His513 to Arg513), the channel forks from the membrane end, creating an extra space above His90 and Arg513. DHDMBFs are seen to occupy lower part of the COX cavity due to their smaller lengths (11.01, 8.04 and 8.06 Å for BF1, BF2 and BF3, respectively) compared to that of the channel (25 Å)¹⁸ and because of electrostatic pull exerted by charged amino acids in the lower part of the COX cavity (Figure 2a).

Interaction energy of BF1 with COX-2 had lowest value, both during energy minimization and molecular dynamics (Table 1). Its higher selectivity may be related to this. However, BF3 had highest volume (1260 Å³) compared to BF2 (1211 Å³) and BF1 (1013 Å³). Higher potency of BF3 compared to BF1 may be due to its larger volume. The result points to the necessity of using a better approach as full free energy perturbation for evaluation of enzyme-inhibitor interac-

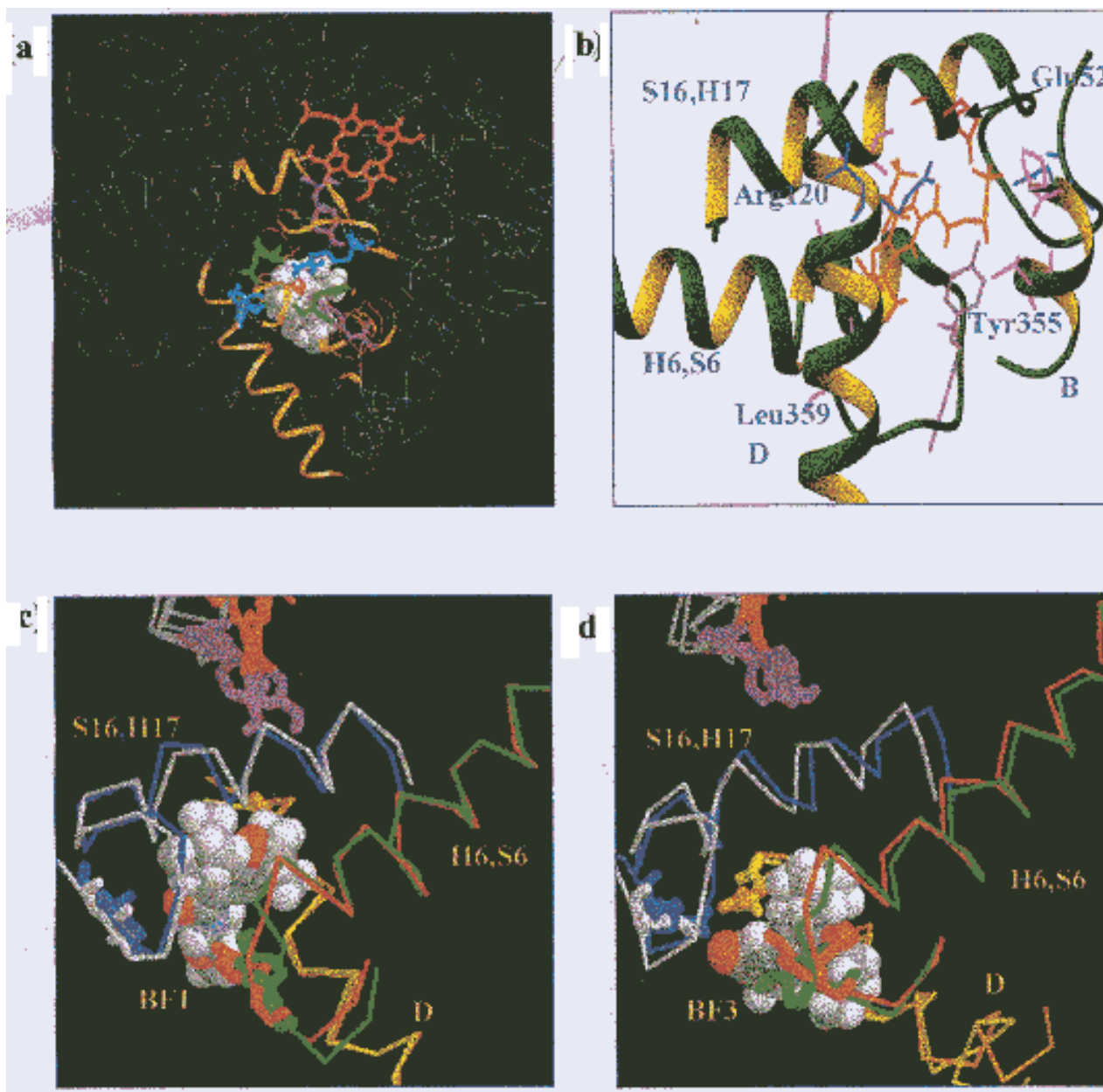


Figure 2. *a*, Energy minimized structure of **BFI** with COX-2. Here the drug is shown in space-fill model, heme-red, neighbouring helices are shown as golden ribbons. Tyr385 at the apex of the channel and Tyr355 at the entrance are shown in purple. Arg120 and Arg513 are cyan. Ser530 is shown in green. The drug resides mostly in the lower part of the cavity; *b*, Closer view of **BFI** in COX-2 cavity. Important side chains and helices are labelled; *c* and *d*, Close view of complexes of **BFI** and **BF3** during molecular dynamics. Snapshots of two trajectories at 180 and 210 ps have been depicted. Tyr385 at the apex of the channel is shown in purple, helices are shown in blue/light blue and green/orange. Helix D is shown in yellow/orange. Drugs shown in space-fill model. One can notice higher mobility of Tyr385 in case of BFI.

tions⁴³. Keeping this in view, we monitored (i) detailed energetics of interaction of DHDMBFs with COX-2; (ii) RMSD of backbone Ca atoms (Figure 3), neighbouring helices and side chains of the protein; (iii) points of contact between DHDMBFs and amino acid chains of COX-2 in the region 1 (hydrophobic region around Tyr385), region 2 (lower part of COX-2 channel) and region 3 (a branch above His90) (Tables 1 and 2, Figure

4). We also monitored H-bonding network at the channel entrance (Table 3).

In case of **BFI**, RMSD of backbone Ca atoms was larger for residues 136–147, which is an inter-domain contact region. The same was noted by us earlier³⁰ in case of NS398, a COX-2-selective ligand. There were series of small peaks in region 325–360 following helix H6 which is adjacent to the active cavity. We also noted

Table 1. Interaction energies (kcal/mole) of DHDMBFs with helical segments and important side chains in catalytic cavity of COX-2 during molecular dynamics (140–250 ps)

Residue range/residue number	BF1	BF2	BF3
COX-2	-43.9	-37.0	-39.4
86–93	-4.5	-2.5	-5.5
106–123	-4.2	-3.4	-7.0
183–195	-0.1	-0.1	-0.1
325–359	-7.2	-6.6	-6.2
379–387	-0.2	-0.1	0.0
426–438	-0.2	-0.1	0.0
509–535	-12.6	-7.5	3.9
Tyr355	-3.2	-2.2	-3.0
Tyr385	-0.1	0.0	0.0
Glu524	-0.4	-0.9	0.0
Arg513	-1.0	-5.3	-2.1
Arg120	-4.7	-4.8	-6.1
His90	-4.6	-1.7	-2.2

Table 2. Points of contact between DHDMBFs and amino acid side chains in energy-minimized model

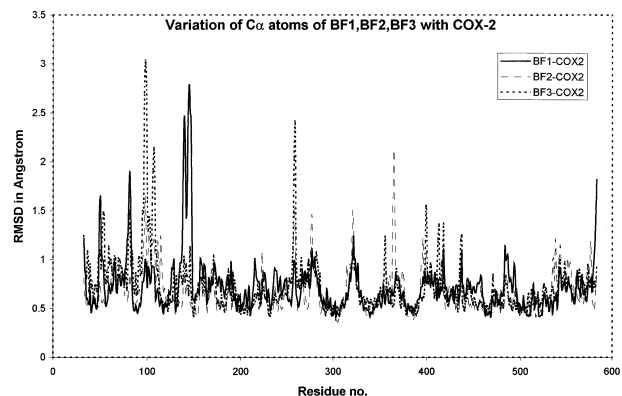
Residue	BF1	BF2	BF3
<i>Region-1</i>			
Val523	-B,R1	-B,R1	-B,R3
Gly526	B-		-
Ala527	B,C B,R3	B,C B,R3	-R3
Ser530	-R3	-R3	-
Leu531	C-	C-	-B,R3
<i>Region-2</i>			
Met	-R2		-
Val116	B,C R1	C R1	C-
Arg120	B,C R1 -B,R3	-R1 C-	C B,R1 -B,R3
Leu352	B,C-	B,C B,R2	C-
Ser353	B,C B,R3	-B,R2	B,C R2
Tyr355	-B,R1,R2 C-	C- -	-B,R1,R2 C-
Glu524	B,C R1	C-	C R1
<i>Region-</i>			
Pro86	B-	-R1	B-
Val89	C R1 -R1	- -R2	C R1 -R1
Arg513	C-	C-	C-

B, Backbone of peptide or benzofuran ring; C, Amino acid side chains of COX; R1, R2, R3 on benzofuran ring as shown in Figure 1.

Summary of H bonding net and Arg513 in DHDMBFs

Residue	Atom	Atom	BF2	BF3	
Arg513	NH1	OE1	✓	✓	
	NH2	OE1	-	✓	
	NH1	OE2	-	✓	
Arg120	Glu524	NH1	OE1	✓	✓
		NH1	OE1	✓	✓
		NH2	OE2	✓	✓

✓ Denotes H-bonding contact for over 50% of simulation period.

**Figure 3.** RMSD of backbone Ca atoms of COX-2 in **BF1**, **BF2** and **BF3**.

comparatively larger RMSD values in the loops 213–220 and 289–295 anchoring heme group in the peroxidase region. Dynamic nature of these loops had been implicated in the second stage of catalysis, viz. conversion of prostaglandin G2 to prostaglandin H2, by Picot *et al.*¹³. However, no significant difference in RMSD values for backbone Ca atoms of Gln203, His207 and His388 involved in heme interaction was noticed. RMSD for side chains of Gln203 and His207 was largest with **BF1**. RMSD for residues 183–195 and 509–535 (helices **S16**, **H17**) around the ligand-binding cavity showed largest value for **BF1**. The latter as well as helix **H6** (residues 325–359) contributed maximum (28 and 16%) to the ligand–protein interaction in **BF1**. These factors seem to be responsible for better COX-2 selectivity by **BF1**.

In case of **BF3**, RMSD for backbone Ca atoms showed few sharp peaks in the region of residues 95–103 which is a membrane-anchoring region. Helices B and D (residues 86–93 and 106–123) in the membrane-anchoring region showed larger RMSD for **BF3** compared to **BF1** and **BF2**. Interaction energies of these two segments with **BF3** were also lower. Larger volume of **BF3** compared to **BF1** and **BF2** contributed to its better interaction with membrane-anchoring region and increased its potency.

In the region 1, contacts between DHDMBFs and COX-2 were predominantly with hydrophobic amino acid residues Val523, Gly526, Ala527 and Leu531 and did not depict any ligand selectivity, except for Gly526. Ser530 did not interact with **BF3**. Tyr385 was much away from the DHDMBFs (Figure 2a) and interacted least. As a result, its side chain showed larger RMSD (0.75–0.92 Å) compared to other residues in the cavity. Largest RMSD value (0.92 Å) was noted in case of **BF1** (Figure 2c and d). Considering strategic location of Tyr385 and its involvement in removal of pro S-hydrogen in arachidonic cascade, its mobility has an important role to play.

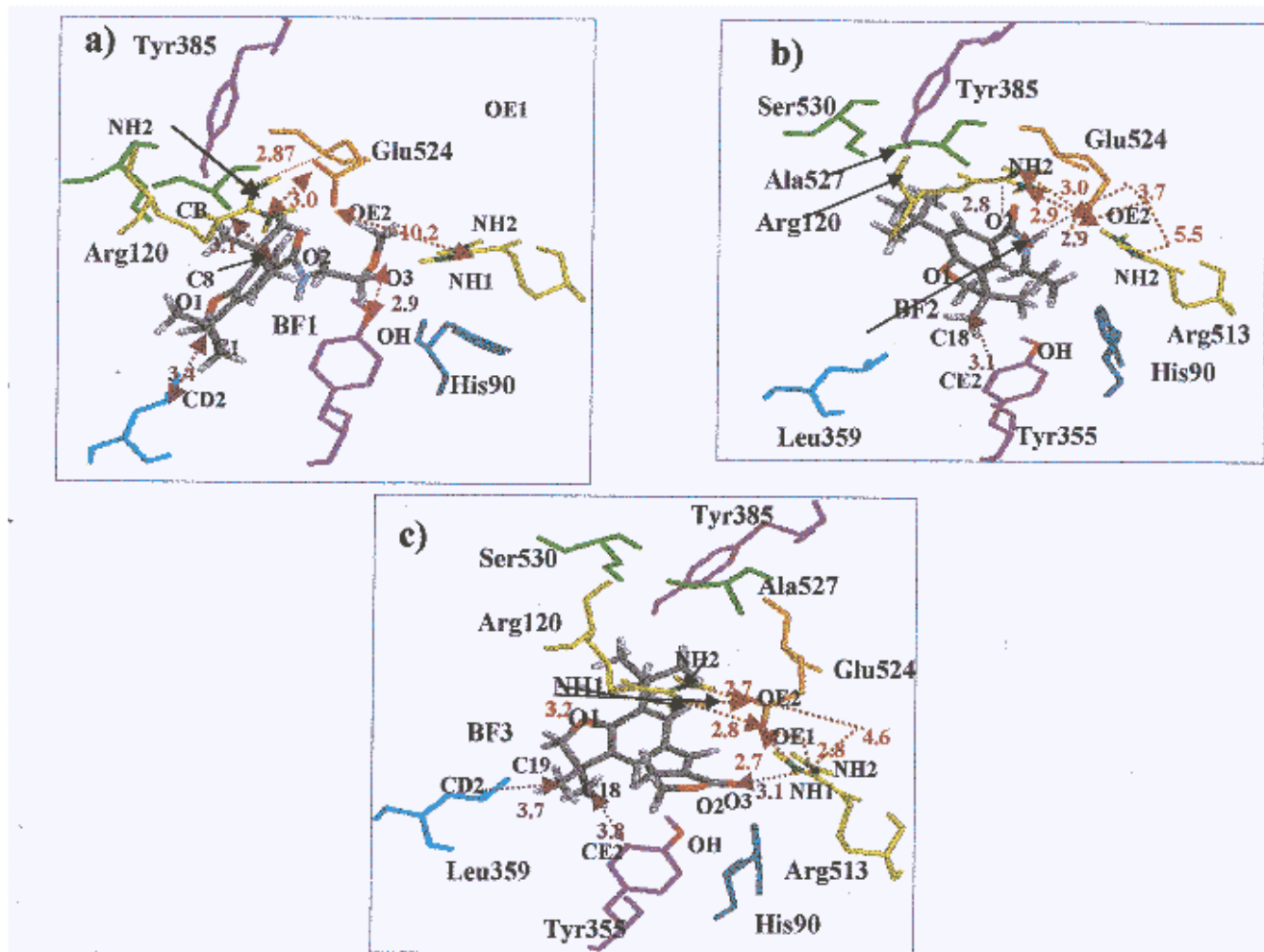


Figure 4a-c. Closer view of BF1, BF2, and BF3 in the active cavity of COX-2 at 180 ps. Residues and helices are labelled. Important distances are shown by dotted lines.

In region 2, carbonyl oxygens of BF1 and BF2 could form H-bonds with Arg120 (Figure 4a and b) for almost 50% of the time, similar to fluorine atom of flurbiprofen. In BF3, although O3 atom in the chain R1 is away from Arg120, the benzofuran ring and *tert*-butyl group in the chain R3 had hydrophobic interaction with Arg120, resulting in its lowest interaction energy (-6.11 kcal/mole) with Arg120. This interaction was nonspecific. Tyr355 formed bifurcated H-bond with O3 of BF1 and a weak H-bond with O3 of BF3. Its interaction energy was lowest with BF1. RMSD for its side chain was largest (1.01 Å) in case of **BF3**. Hydrogen bond is observed between side chain of Glu524 and N1H atoms of BF2 (Figure 4b). As a result, interaction energy of Glu524 with BF2 was lower compared to that with BF1 and BF3. In the latter case, a weak hydrogen bond is seen between C9H and OE1 of Glu524. O3 atom of BF3 approaches a distance of 2.86 Å with OE1 of Glu524, which may form water-mediated H-bond. Met113 interacted only in the case of **BF1**. Hydrophobic residues Val116, Val349, Leu352 and neutral polar

residues Ser353 have very good interactions with the benzofuran core and side chains R2 and R3 in case of all the three ligands.

In region 3, H-bonding and electrostatic interactions were noticed for side chain of Arg513 with O3 atoms of BF1 and BF3 (Figure 4a and c). These interactions were absent in **BF2** in the energy-minimized model (Figure 4b). However, during molecular dynamics, Arg513 moved towards BF2 and had lowest interaction energy with BF2. RMSD for backbone Ca atoms and side chain of Arg513 had highest value (0.73 Å) for **BF3**. His90 also had H-bonding interaction with BF1, leading to lowest interaction energy (-4.6 kcal/mole) during simulations. We find good interaction of Pro86 and Val89 with chain R1 in case of **BF1** and **BF3**.

Perturbations in the COX-2 structures at the channel entrance

On the basis of kinetic data on mutation of Tyr355-Phe355, it had been proposed by So *et al.*²⁸ that con-

formational changes at the entrance of the channel restricted by the H-bonding network amongst Arg513/Glu524/Tyr355, and Arg120/Glu524/Tyr355 may give rise to a rate-limiting process and COX-2 selectivity by some ligands. To examine this hypothesis we monitored inter-atomic distances amongst backbone atoms CO, NE, NH1 and NH2 of Arg120 and Arg513, CO, OE1 and OE2 of Glu524 and CO and OH of Tyr355 during the simulation. It was seen that Tyr355 remained at a distance from Arg513, Glu524 and Arg120. This was because of its strong interaction with the DHDMBFs (Table 1, Figure 4 a–c). Arg120 and Arg513 showed good interaction with Glu524 in complexes **BF2** and **BF3** (Figure 4 b and c, Table 3). The conformation at the channel entrance in these two cases was ‘partially open’. In case of **BF1**, Arg513 interacted with the ligand and could not form H-bonds with Glu524. The conformation at the channel entrance was more ‘relaxed’ compared to **BF2** and **BF3** (Figure 4 a). The distance between side chains of Arg513 and Glu524 was larger than 10 Å. Similar pattern was seen in X-ray data on SC558-COX2 (ref. 17) and molecular dynamics simulation results on NS398-COX-2 complex³⁰. The reason for more ‘relaxed’ conformation at the channel entrance in case of **BF1**, NS398 and SC558 is bulkiness at the lower part of these ligands. Interaction between SO₂ of NS398 or SC558 and O2 and O3 of **BF1** with Tyr355 and Arg513 facilitated ‘relaxed’ conformation at the channel entrance. This result was in agreement with the kinetic model of So *et al.*²⁸ for COX-2 selectivity. The non-selective ligands like flurbiprofen¹⁷ and indoprofen³⁰ led to more ‘tight’ conformation.

Summary and conclusion

Molecular dynamics simulation results on **BF1**, **BF2** and **BF3** with COX-2 showed that **BF1** leads to larger mobility of backbone C α atoms of residues 136–147 in interdomain contact region, residues 213–220 and 289–295 in loops adjacent to heme group and side chains of residues Glu203 and His207 involved in the interaction with heme. The side chain of Tyr385 was also more flexible. There was stronger interaction with helical segment residues 509–535 and 325–359 around the cavity. Arg120, Tyr355, Arg513 and His90 had H-bonding and electrostatic interaction with **BF1**. As a result, Tyr355 and Arg513 are pulled towards **BF1**, breaking the H-bond between Glu524 and Arg513. This leads to a more ‘relaxed’ conformation at the channel entrance. In addition, there were hydrophobic contacts with Met113, Pro86 and Val89. Higher COX-2 selectivity by **BF1** may be due to combined effect of all these interactions.

Higher potency of **BF3** is possibly due to its better interaction with the membrane anchoring helices B and D because of its larger volume. **BF3** had strong, but

non-specific interaction with Arg120 during molecular dynamics. RMSD of residues Tyr355 and His90 in the lower part of the cavity was largest for **BF3**. The channel in case of **BF2** and **BF3** was ‘partially open’ due to H-bonding network amongst Arg120, Glu524 and Arg513.

Thus COX-2 selectivity is related to specific H-bonding and electrostatic and few hydrophobic interactions in the lower part of the channel. These lead to a ‘relaxed’ conformation at the channel entrance. While potency seems to be related to interactions with membrane-anchoring region at one end and Tyr385 at the apex of the channel. Replacing *tert*-butyl group of DHDMBFs by a benzene ring with carbonyl, sulphate or nitrate would yield better contact with Tyr385 at the apex of the channel, which also would enhance activity.

1. Janusz, J. M. *et al.*, *J. Med. Chem.*, 1998, **41**, 1112–1123.
2. Janusz, J. M. *et al.*, *J. Med. Chem.*, 1998, **41**, 3515–3529.
3. Holtzman, M. J., Turk, J. and Shornick, L. P., *J. Biol. Chem.*, 1992, **267**, 21438–21445.
4. Masferrer, J. L., Seibert, K., Zweifel, B. and Needleman, P., *Proc. Natl. Acad. Sci. USA*, 1992, **89**, 3917–3921.
5. O’Banion, M. K., Sadowski, H. B., Winn, V. and Young, D. A., *J. Biol. Chem.*, 1991, **266**, 23261–23267.
6. Meade, E. A., Smith, W. L. and DeWitt, D. L., *J. Biol. Chem.*, 1993, **268**, 6610–6614.
7. Herschman, H. R., *Biophys. Acta*, 1996, **1299**, 125–140.
8. Seibert, K. *et al.*, *Proc. Natl. Acad. Sci. USA*, 1994, **91**, 12013–12017.
9. Masferrer, J. L. *et al.*, *Proc. Natl. Acad. Sci. USA*, 1994, **91**, 3228–3232.
10. Dewitt, D. L., el-Harith, E. A., Kraemer, S. A., Andrews, M. J., Yao, E. F., Armstrong, R. L. and Smith, W. L., *J. Biol. Chem.*, 1990, **265**, 5192–5198.
11. Smith, W. L. and Marnett, L. J., in *Metal Ions in Biological Systems* (eds Sigel, H. and Sigel, A.), Marcell Dekker, New York, 1994, pp. 163–199.
12. Smith, W., Garavito, R. and DeWitt, D., *J. Biol. Chem.*, 1996, **271**, 33157–33160.
13. Picot, D., Loll, P. J. and Garavito, R. M., *Nature*, 1994, **367**, 243–249.
14. Loll, P., Picot, D. and Garavito, R., *Nat. Struct. Biol.*, 1995, **2**, 637–643.
15. Loll, P., Picot, D. and Garavito, R., *Biochemistry*, 1996, **35**, 7330–7340.
16. Luong, C., Miller, A., Barnett, J., Chow, J., Ramesha, C. and Browner, M. F., *Nat. Struct. Biol.*, 1996, **3**, 927–933.
17. Kurumbail, R. G. *et al.*, *Nature*, 1996, **384**, 644–648.
18. Garavito, R. M., *Nat. Struct. Biol.*, 1996, **3**, 897–901.
19. Bhattacharyya, D. K., Lecomte, M., Rieke, C. J., Garavito, R. M. and Smith, W. L., *J. Biol. Chem.*, 1996, **271**, 2179–2184.
20. Smith, W. L., Eling, T. E., Kulmacz, R. J., Marnett, L. J. and Tsai, A., *Biochemistry*, 1992, **31**, 3–7.
21. Dietz, R., Nastainczyk, W. and Ruf, H. H., *Eur. J. Biochem.*, 1988, **171**, 321–328.
22. Guo, Q., Wang, L. H., Ruan, Ke-He. and Kulmacz, R. J., *J. Biol. Chem.*, 1996, **271**, 19134–19139.
23. Wong, E., Bayly, C., Waterman, H. L., Reienbeau, D. and Mancin, J. A., *Biol. Chem.*, 1997, **272**, 9280–9286.
24. Rome, L. H. and Lands, W. E. M., *Proc. Natl. Acad. Sci. USA*, 1975, **72**, 4863–4865.
25. Kulmacz, R. J. and Lands, W. E. M., *J. Biol. Chem.*, 1985, **260**, 12572–12678.

26. Copeland, R. A. *et al.*, *Proc. Natl. Acad. Sci. USA*, 1994, **91**, 11202–11206.
27. Swinney, D. C., Mak, A. Y., Barnett, J. and Ramesha, C. S., *J. Biol. Chem.*, 1997, **272**, 12393–12398.
28. So On-Yee., Scarafia, E. E., Mak, A. Y., Callan, O. H. and Swinney, D. C., *J. Biol. Chem.*, 1998, **273**, 5801–5807.
29. Kothekar, V., Sahi, S. and Srinivasan, M., *J. Biomol. Struct. Dyn.*, 1999, **16**, 901–915.
30. Sahi, S., Srinivasan, M. and Kothekar, V., *J. Mol. Struct. (Theor. Chem)*, 2000, **498**, 133–148.
31. Du Pont, L., *Acta Cryst.*, 1995, **C51**, 507–509.
32. Stewart, J. J. P., MOPAC 7.0 QCPE Bloomington, IN. USA, 1993.
33. Kothekar, V., Sahi, S. and Mishra, J., *Indian J. Biochem. Biophys.*, 1999, **35**, 273–283.
34. Protein Data Bank, Chemistry Department Building, 555 Brookhaven National Laboratory, P.O. Box 5000 USA.
35. Koradi, R. MOLMOL – A molecule analysis and display program, Institut fur Molekular Biology und Biophysik, ETH, Zurich, Spectrospin AG, Fallenden, Switzerland, 1997.
36. Kothekar, V. and Mrigank, *Phys. Educ.*, 1988, **5**, 169–176.
37. Case, D. A. *et al.*, AMBER 5.0: Assisted Model Building with Energy Refinement – A Computer Simulation Software developed by the University of California, USA, 1997.
38. Fletcher, R. and Reeves, C. M., *Comput. J.*, 1964, **7**, 149–154.
39. Sayle, R. A., RASMOL – Molecular Visualization Program Glaxo Research and Development, Greenfield, Middlesex, UK, 1994.
40. Verlett, L., *Phys. Rev.*, 1967, **130**, 98–103.
41. Hockney, R. W. and Eastwood, J. W., in *Computer Simulations using Particles*, McGraw Hill, New York, 1981.
42. Jorgenson, W. L., Chandrasekhar, J., Medura, J. D., Impey, R. W. and Klein, M. L., *J. Chem. Phys.*, 1983, **79**, 926–935.
43. Kollman, P., *Pharm. Res.*, 1998, **15**, 368–370.

ACKNOWLEDGEMENTS. We thank Department of Science and Technology for financial assistance. S.S. is thankful to Council of Scientific and Industrial Research for award of Senior Research fellowship.

Received 21 September 2000; revised accepted 17 January 2001

RESEARCH COMMUNICATIONS

Effect of glycosylation on iron-mediated free radical reactions of haemoglobin

Manoj Kar* and Abhay S. Chakraborti^{†, #}

*Department of Biochemistry, Nilratan Sarkar Medical College Hospital, Kolkata 700 014, India

[†]Department of Biophysics, Molecular Biology and Genetics, University of Calcutta, 92 APC Road, Kolkata 700 009, India

HbA_{1c}, the major glycosylated haemoglobin increases proportionately with blood glucose level in diabetes mellitus. Here we demonstrate that H₂O₂-induced iron release is more from HbA_{1c} than that from non-glycosylated haemoglobin (HbA₀). In the presence of H₂O₂, HbA_{1c} degrades arachidonic acid and deoxyribose more efficiently than HbA₀, which suggests that iron release is more with HbA_{1c} compared to HbA₀. Increased rate of oxidation of HbA_{1c} in the presence of nitrobluetetrazolium is indicated by an increase in methaemoglobin formation. HbA_{1c} exhibits less peroxidase activity than HbA₀. These findings on glycosylation-induced functional properties of haemoglobin suggest a mechanism of increased formation of free radicals and oxidative stress in diabetes mellitus.

IN diabetes mellitus, oxidative stress is associated with increased production of reactive oxygen species (ROS) like superoxide radical, hydroxyl radical or hydrogen peroxide^{1–3}. ROS is responsible for tissue damaging

effect, leading to pathophysiological complications^{4,5}. The mechanism of increased formation of free radicals in diabetes mellitus is still not clear, but prevailing theory suggests that a reduced level of scavenging enzymes like superoxide dismutase, glutathione reductase^{6,7} and deficiencies of antioxidants like vitamins E and C (refs 8–10) stimulate free radical formation in this pathological condition.

Allen *et al.*¹¹ in 1958 first reported the existence of several glycosylated haemoglobin species (HbA_{1a}, HbA_{1b}, HbA_{1c}) in minor amounts in normal human blood. Of these species, HbA_{1c}, in which glucose is linked to N-terminal valine residues of *b* chains, is of utmost importance as its formation is increased in diabetic patients with ambient hyperglycemia and is used to monitor clinically for long-term control of blood sugar¹². In normal physiological state, iron is tightly bound within protoporphyrin ring of heme pocket. Under specific circumstances, iron is released from heme and ligated to another moiety, perhaps the distal histidine in the heme pocket. This iron termed 'free reactive iron' can be detected by ferrozine reaction¹³.

Recently, we have reported¹⁴ that free reactive iron level in purified haemoglobin (total) isolated from blood of diabetic patients is proportionately increased with increased level of blood glucose. Since iron may be a source of free radicals, it may explain increased formation of free radicals and oxidative stress in diabetes mellitus. However, there has been no study on glycosylated haemoglobin-induced iron release and free radical-mediated biochemical reactions. This has led us to isolate nonglycosylated (HbA₀) and glycosylated haemoglobin (HbA_{1c}) from blood samples of diabetic

[#]For correspondence (e-mail aschak@cubmb.ernet.in)